

Supporting Information

Metal-Free Half-Metallicity in a High Energy Phase C-doped gh-C₃N₄ System: A High Curie Temperature Planar System.

Indrani Choudhuri,[†] Gargee Bhattacharyya,[#] Sourabh Kumar,[†] Biswarup Pathak,^{†,#,*}

[†]Discipline of Chemistry and [#]Discipline of Metallurgy Engineering and Materials Science,
Indian Institute of Technology (IIT) Indore, Indore. M.P. 453552, India

Email: biswarup@iiti.ac.in

Contents:

Text S1. Formation Energy (E_f) and Binding Energy (E_B) calculations.

Table S1: Formation energy (E_f) and binding energy (E_B/C), magnetic moments and types of C doped gh-C₃N₃ with different C-doping concentration and doping position.

Figure S1: (a) Optimized structure, TDOS/PDOS and Band Structure of C_{N1}@gh-C₃N₄. (b) Optimized structure, TDOS/PDOS and Band Structure of C_{N3}@gh-C₃N₄. A red dashed box shows unitcell. The Fermi level is indicated by a black dashed line.

Figure S2: Total and partial DOS of C_{N2}@gh-C₃N₄ using HSE06 functional.

Figure S3: Partial DOS of (a) C_{N1}@gh-C₃N₄, (b) C_{N2}@gh-C₃N₄ and (c) C_{N3}@gh-C₃N₄.

Figure S4: Schematic representation of sp² hybridization in C_N@gh-C₃N₄.

Figure S5: The structure of (a) pure gh-C₃N₄, (b) C_{N1}@gh-C₃N₄, (c) C_{N2}@gh-C₃N₄, and (d) C_{N3}@gh-C₃N₄. The black dashed circle denotes the doped C-atom.

Figure S6: Electrostatic potentials (ESP) plots (Isosurface value: $0.09 \text{ e.}\text{\AA}^{-3}$) of (a) pure gh-C₃N₄, (b) C_{N1}@gh-C₃N₄, (c) C_{N2}@gh-C₃N₄, and (d) C_{N3}@gh-C₃N₄. The blue and red colours denote less and more electron dense area in the electrostatic potential surface.

Figure S7: Optimized structures and total and partial density of states of 3.12% (a) C_{N1}@gh-C₃N₄, (b) C_{N2}@gh-C₃N₄, and (c) C_{N3}@gh-C₃N₄ systems. A red dashed box shows unitcell.

Figure S8: Optimized structures and total and partial density of states of 6.25% (a) C_{N1}@gh-C₃N₄, (b) C_{N2}@gh-C₃N₄, and (c) C_{N3}@gh-C₃N₄ systems. A red dashed box shows unitcell.

Figure S9: Optimized structures and total and partial density of states of 9.37% (a) C_{N1}@gh-C₃N₄, (b) C_{N2}@gh-C₃N₄, and (c) C_{N3}@gh-C₃N₄ systems. A red dashed box shows unitcell.

Figure S10: Total energy fluctuation during AIMD simulations of (a) C_{N1}@gh-C₃N₄, and (b) C_{N3}@gh-C₃N₄ systems at 500 and 1000 K. The structures represent the snapshot at 10 ps for each simulation.

Text S2: Calculation of mechanical properties

Table S3: Exchange energy (E_{ex}) and Curie temperature (T_C) value of 12.50% C_N@gh-C₃N₄ system.

Text S3. Calculation of Magnetic Anisotropy Energy (MAE)

References

=====

Text S1. Formation Energy (E_f) and Binding Energy (E_B) Calculations

The formation energy (E_f) is calculated for each C-doped gh-C₃N₄ using the following equation:

$$E_f = (E_{C(N)@gh-C_3N_4} - E_{gh-C_3N_4}) - x(\mu_C - \mu_N) \quad (2)$$

where $E_{C(N)@gh-C_3N_4}$ is the total energy of C_N@gh-C₃N₄, $E_{gh-C_3N_4}$ is the total energy of gh-C₃N₄ sheet. μ_C and μ_N represents the chemical potential of carbon and nitrogen atoms, which are calculated from graphene and N₂, respectively. We have also calculated the binding energy (E_B) of carbon in the N-site of gh-C₃N₄ using the following equation:

$$E_B = E_{CN@gh-C_3N_4} - (E_{gh-C_3N_4} + xE_C) \quad (3)$$

where, E_C represents the total energy of the isolated C atom.

Table S1: Formation energy (E_f)/dopant, binding energy (E_B), magnetic moments (per doped C), Band gap (eV) for C_N@gh-C₃N₄ systems are tabulated. Different doping C-concentrations and their respective values are given.

Doping concentration (%)	E_f (eV)	E_B (eV)	Magnetic moment (μ_B)	Nature	Band gap (eV)	
3.12	N1-position	0.52	8.72	0.90	Metallic	--
	N2-position	1.05	9.06	1.00	Semiconductor	0.92
	N3-position	0.41	8.83	0.80	Metallic	--
6.25	N1-position	0.56	8.68	0.90	Metallic	--
	N2-position	1.09	9.04	1.00	Semiconductor	0.86
	N3-position	0.45	8.81	0.80	Metallic	--
9.37	N1-position	0.56	8.53	0.90	Metallic	--
	N2-position	1.02	9.17	1.00	Semiconductor	0.59
	N3-position	0.42	8.72	0.80	Metallic	--
12.50	N1-position	0.55	8.44	0.90	Semiconductor	Up-spin: 1.98 Down-spin: 0.33
	N2-position	1.12	9.12	1.00	Half-metallic	Up-spin: Metallic Down-spin: 1.45
	N3-position	0.43	8.67	0.80	Semiconductor	Up-spin: 2.10 Down-spin: 0.13

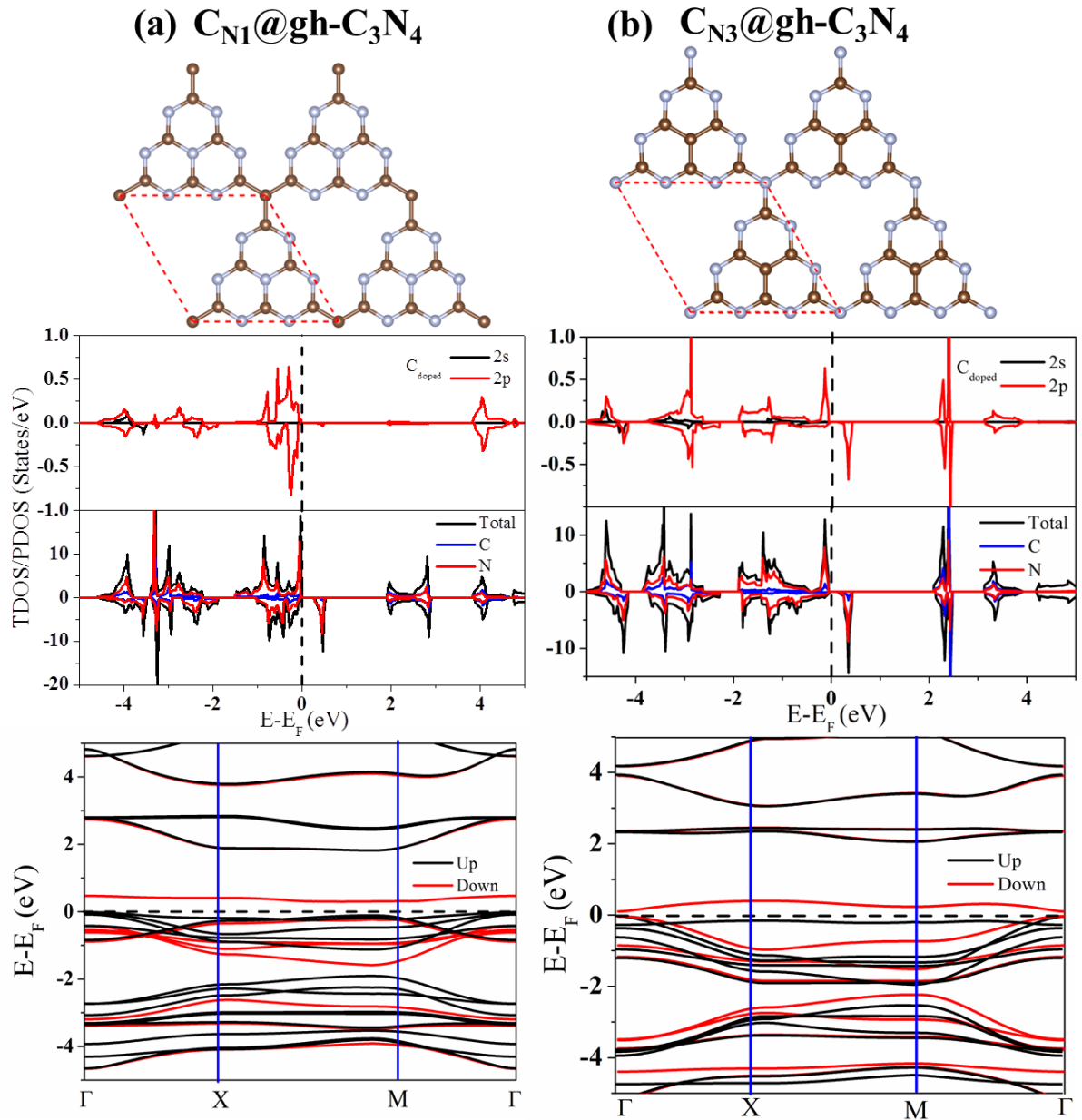


Figure S1: (a) Optimized structure, TDOS/PDOS and Band Structure of C_{N1}@gh-C₃N₄. (b) Optimized structure, TDOS/PDOS and Band Structure of C_{N3}@gh-C₃N₄. A red dashed box shows unitcell. The Fermi level is indicated by a black dashed line.

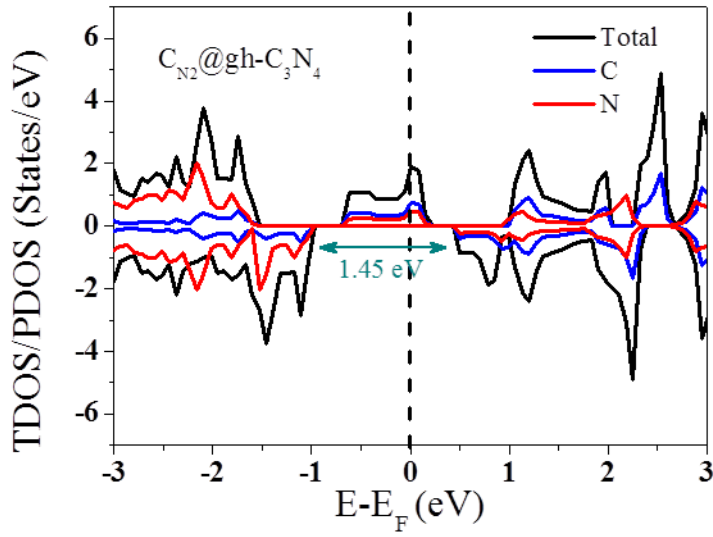


Figure S2: Total and partial DOS of $C_{N2}@gh-C_3N_4$ using HSE06 functional.

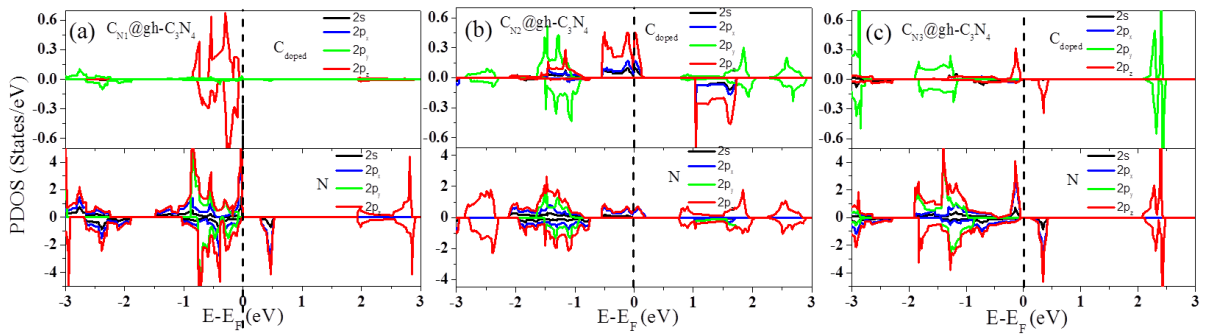


Figure S3: Partial DOS of (a) $C_{N1}@gh-C_3N_4$, (b) $C_{N2}@gh-C_3N_4$ and (c) $C_{N3}@gh-C_3N_4$.

sp^2 Hybridization of C_{doped} in 12.50% $C_N@gh-C_3N_4$

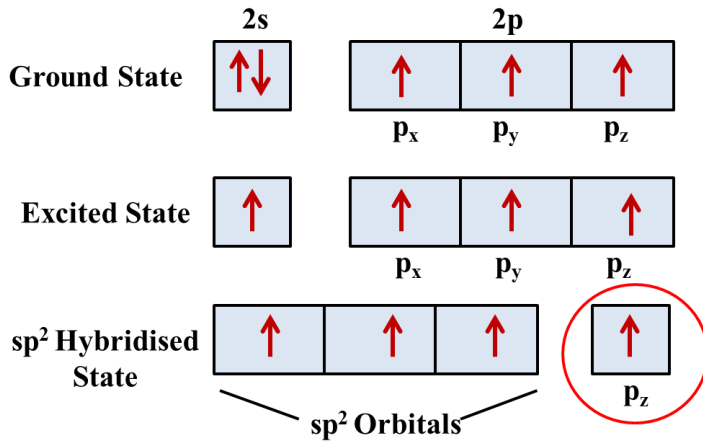


Figure S4: Schematic representation of sp^2 hybridization in $C_N@gh-C_3N_4$.

Table S2: Bader charges of $C_N@gh-C_3N_4$ systems.

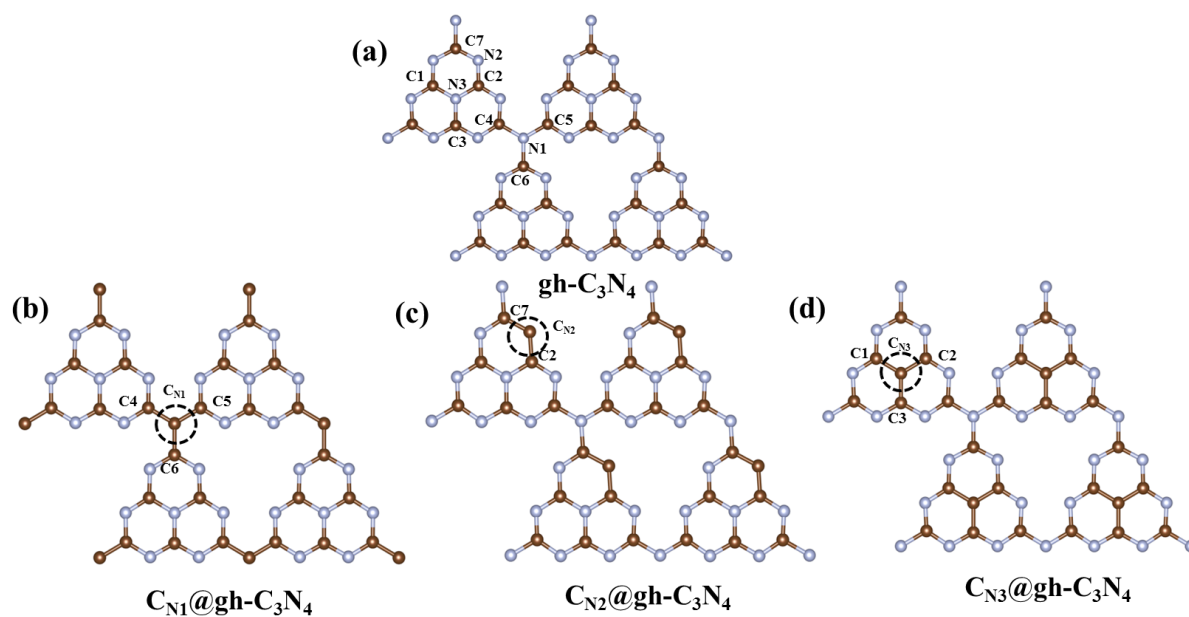


Figure S5: The structure of (a) pure $gh-C_3N_4$, (b) $C_{N1}@gh-C_3N_4$, (c) $C_{N2}@gh-C_3N_4$, and (d) $C_{N3}@gh-C_3N_4$. The black dashed circle denotes the doped C-atom.

System	Net Effective Charges	
	C	N
$gh-C_3N_4$	C1= +1.75 C2=C3= +1.42 C4= +1.64 C5=C6=C7=+1.37	N1= -1.03 N2= -1.07 N3= -1.17
$C_{N1}@gh-C_3N_4$	C4=C5=C6= +1.06 C _{N1} = +0.25	N2= -1.15 N3= -1.09
$C_{N2}@gh-C_3N_4$	C2=+0.84 C7=+0.83 C _{N2} = +0.26	N1= -1.08 N3= -1.23
$C_{N3}@gh-C_3N_4$	C1=C2=C3=+1.04 C _{N3} = +0.14	N1= -1.11 N2= -1.13

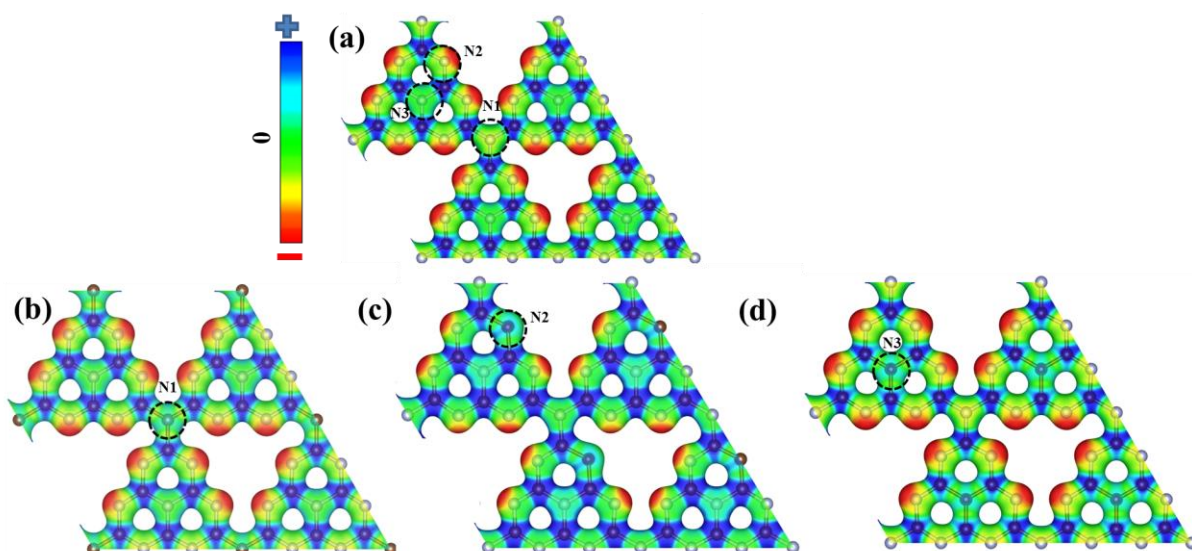


Figure S6: Electrostatic potentials (ESP) plots (Isosurface value: $0.09 \text{ e} \cdot \text{\AA}^{-3}$) of (a) pure gh- C_3N_4 , (b) C_{N_1} @gh- C_3N_4 , (c) C_{N_2} @gh- C_3N_4 , and (d) C_{N_3} @gh- C_3N_4 . The blue and red colours denote less and more electron dense area in the electrostatic potential surface.

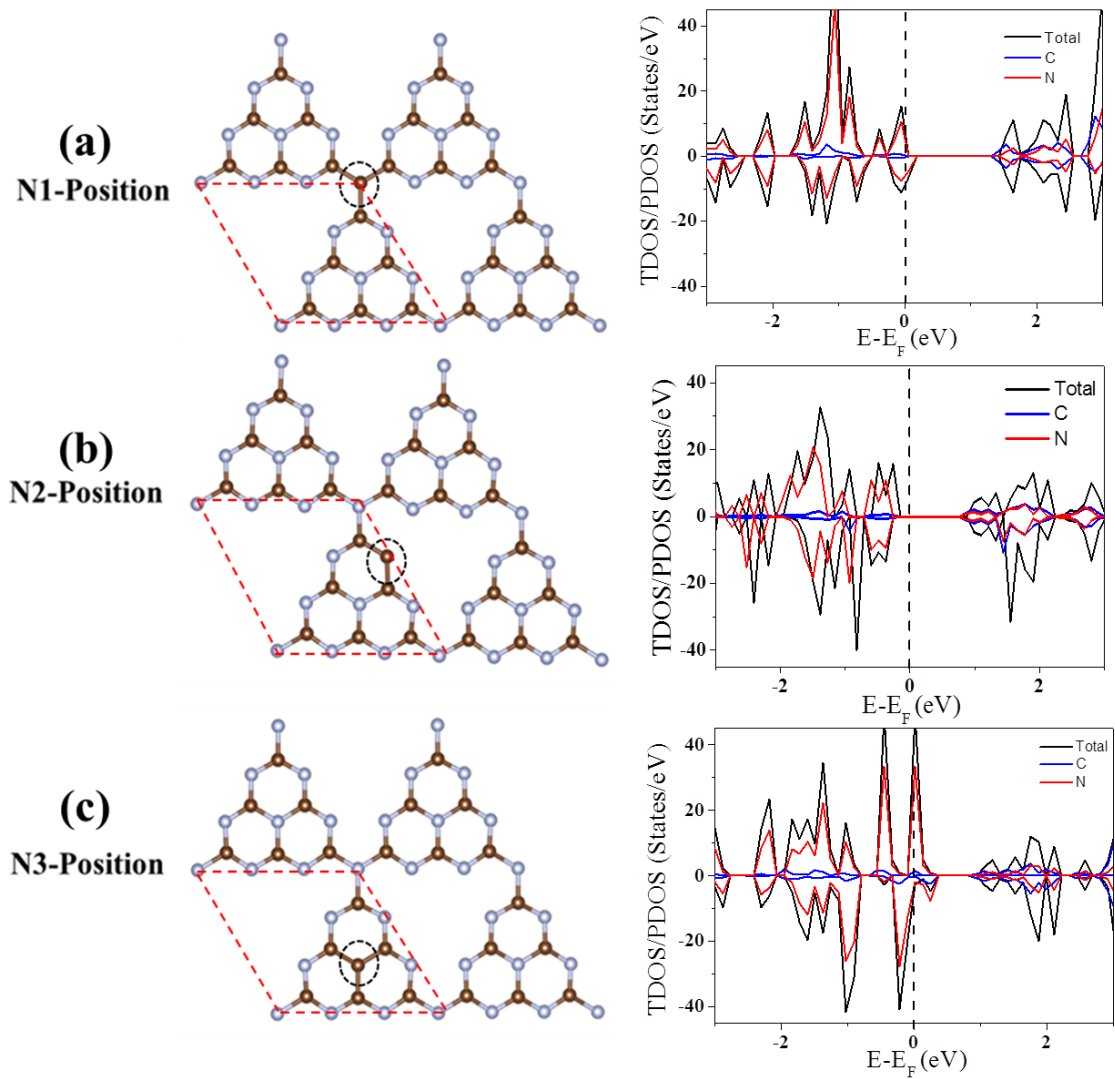


Figure S7: Optimized structures and total and partial density of states of 3.12% (a) $C_{N1}@gh-C_3N_4$, (b) $C_{N2}@gh-C_3N_4$, and (c) $C_{N3}@gh-C_3N_4$ systems. A red dashed box shows unitcell.

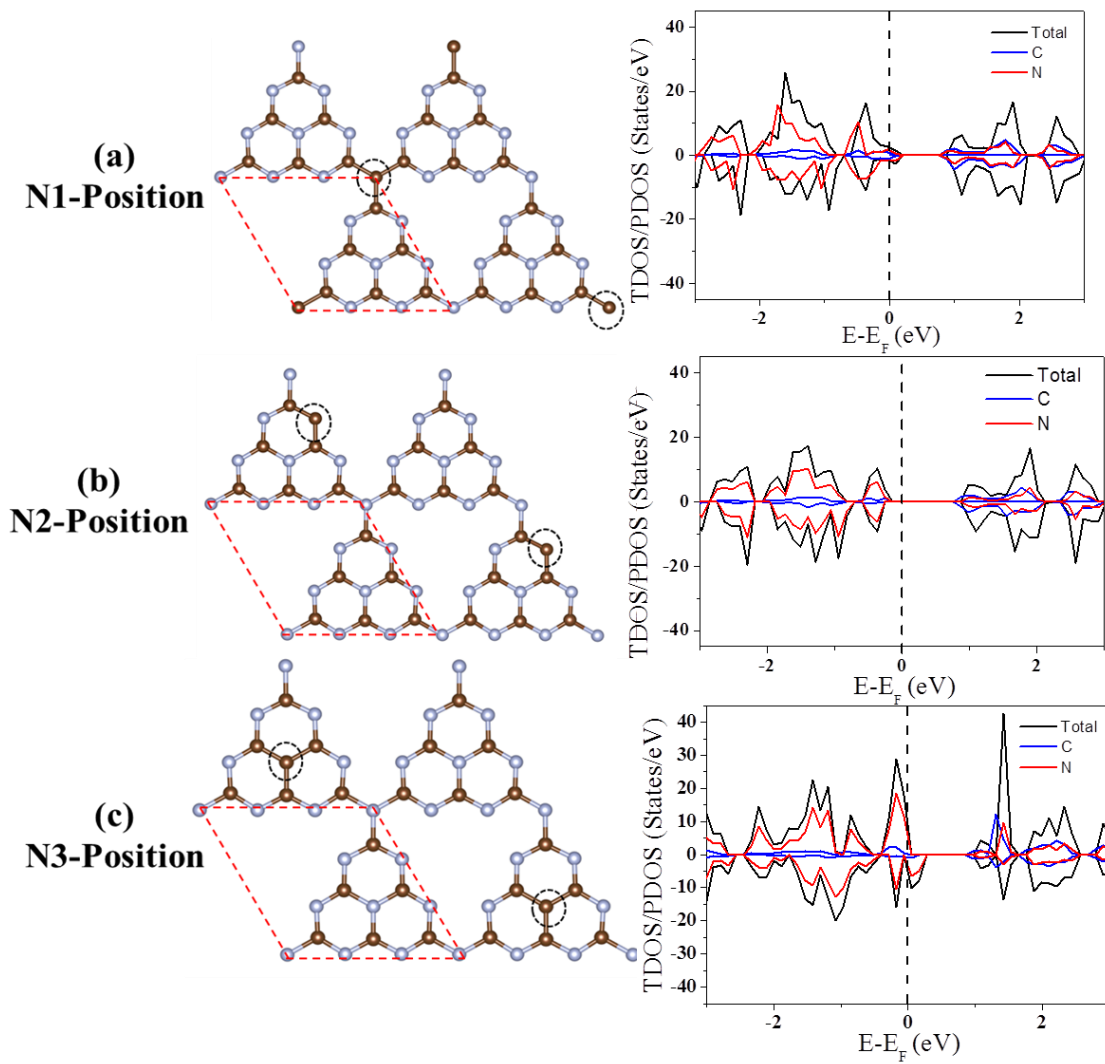


Figure S8: Optimized structures and total and partial density of states of 6.25% (a) $C_{N1}@gh-C_3N_4$, (b) $C_{N2}@gh-C_3N_4$, and (c) $C_{N3}@gh-C_3N_4$ systems. A red dashed box shows unitcell.

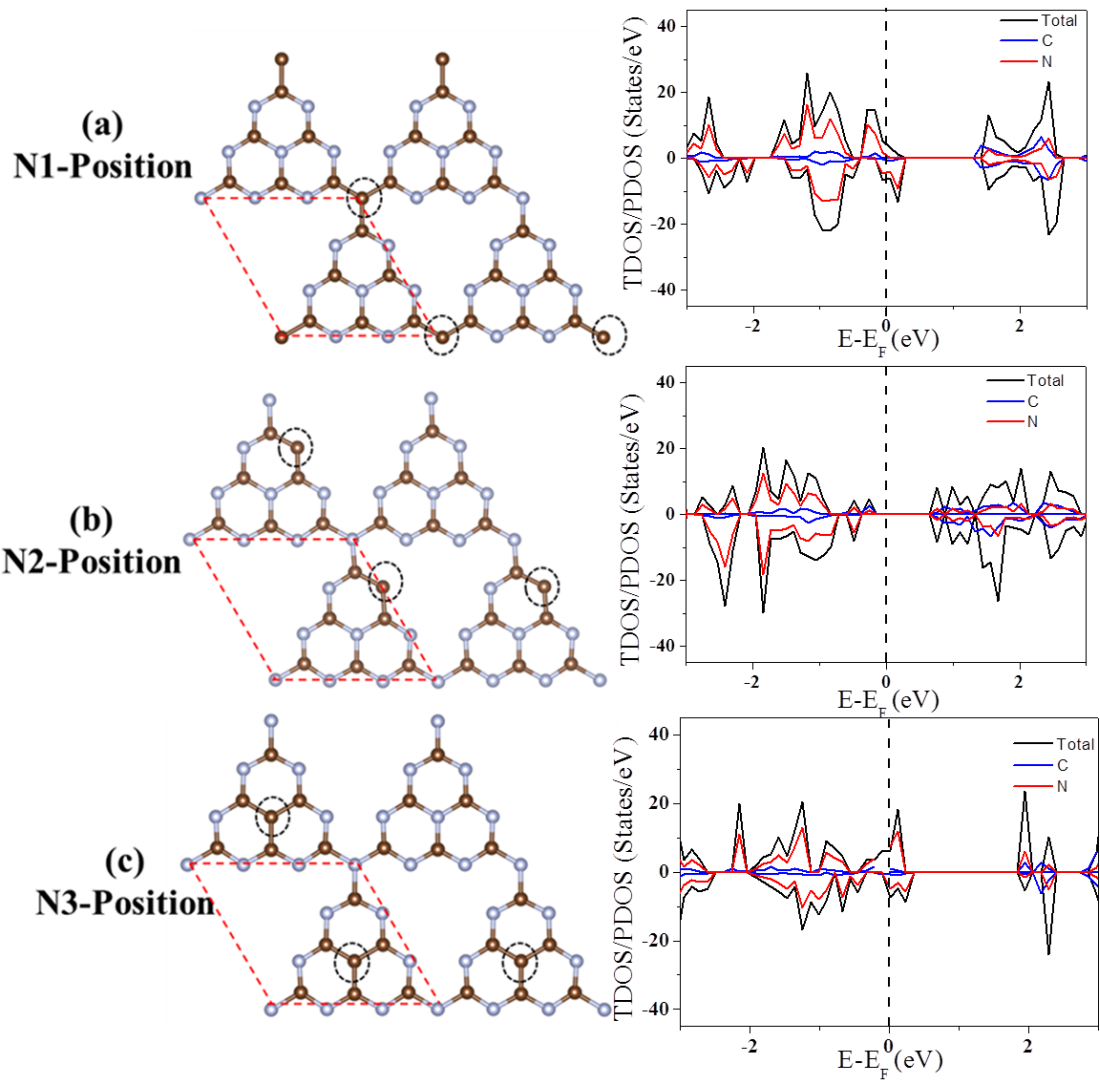


Figure S9: Optimized structures and total and partial density of states of 9.37% (a) $C_{N1}@gh-C_3N_4$, (b) $C_{N2}@gh-C_3N_4$, and (c) $C_{N3}@gh-C_3N_4$ systems. A red dashed box shows unitcell.

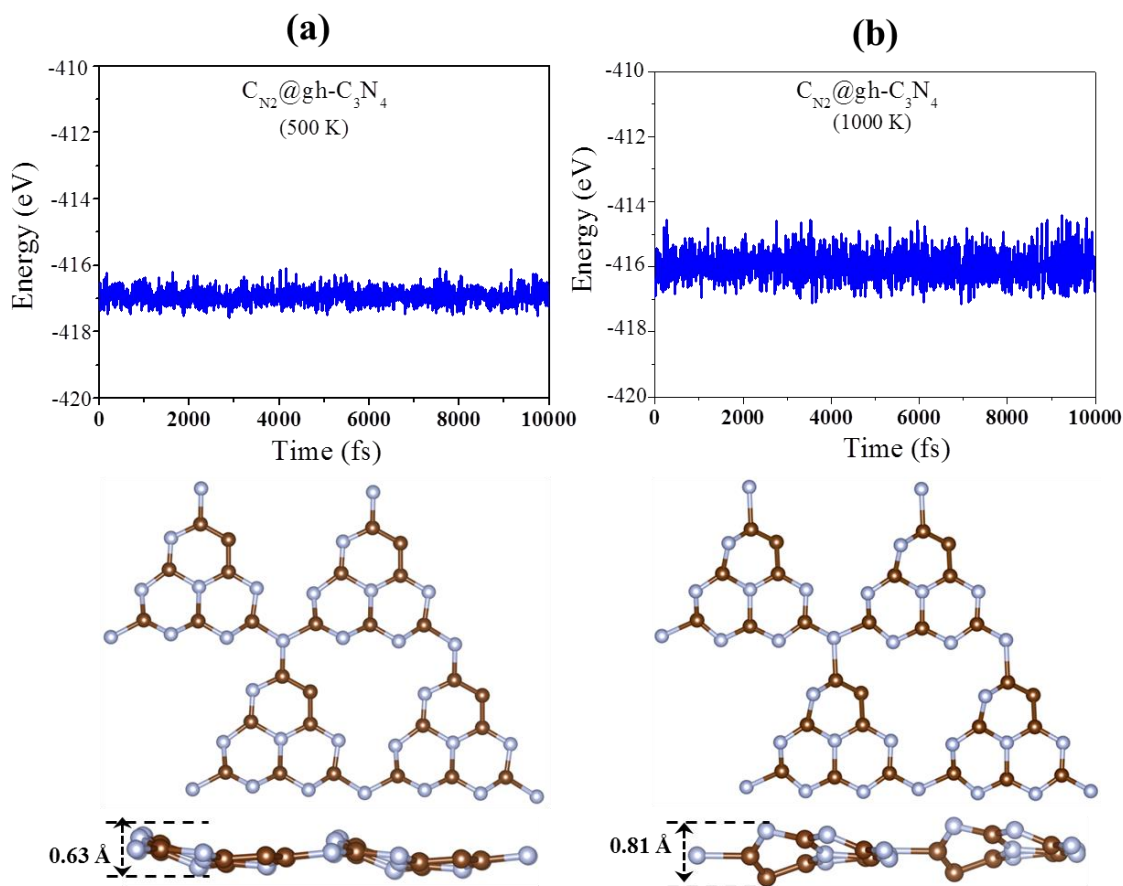


Figure S10: Total energy fluctuation during AIMD simulations of (a) $C_{N_1}@gh-C_3N_4$, and (b) $C_{N_3}@gh-C_3N_4$ systems at 500 and 1000 K. The structures represent the snapshot at 10 ps for each simulation.

Text S2: Calculation of mechanical properties

The $C_{N_2}@gh-C_3N_4$ monolayer sheets can be distorted either by tensile strain (by gradually increasing the lattice parameters) or compressive strain (by gradually reducing the lattice parameters). The percentage (%) of applied strain can be calculated as follows.¹

$$\% \text{ Strain} = (a - a_1) / a \times 100 \quad (4)$$

Here ‘a’ and ‘a₁’ are the lattice constants of the monolayer sheet before and after the strain. Tensile strains are applied along the in-plane uniaxial and biaxial directions to calculate the mechanical stability of $C_{N_2}@gh-C_3N_4$ system. The effects of uniaxial and biaxial strains are

examined on a supercell (2×2×1) of 56 atoms. Atomic positions are relaxed at each strain until the forces on each atom are less than 10⁻² eV/Å. Elastic limit is calculated from the stress-strain curve under the tensile stretch given in the manuscript in Figure 4c.²

Further, the mechanical properties of the C_{N2}@gh-C₃N₄ sheets can be calculated from the strain vs. strain energy plot [Figure 4b, Manuscript]. The elastic energy (U/per unit cell) near the equilibrium position can be calculated using the following formula:

$$U = \frac{1}{2}C_{11}\varepsilon_{xx}^2 + \frac{1}{2}C_{22}\varepsilon_{yy}^2 + C_{12}\varepsilon_{xx}\varepsilon_{yy} + 2C_{44}\varepsilon_{xy}^2 \quad (5)$$

where, C₁₁, C₂₂, C₁₂ and C₄₄ are the linear elastic constants, whereas ε_{xx}, ε_{yy}, ε_{xy} are the in-plane stress along the x, y and xy directions (according to Voigt notation),⁴ respectively. The value of the elastic constants can be calculated from the polynomial fitting of strain vs. energy plot.⁴⁻⁶ The main criteria for mechanical stability are C₁₁ > C₁₂ and C₄₄ > 0. The value of C₁₁ can be obtained under uniaxial deformation, whereas C₁₂ can be calculated by polynomial fitting under biaxial deformation. For all three C_{N2}@gh-C₃N₄ systems, we find that C₁₁ > C₁₂ and C₄₄ > 0. Thereby, the calculated elastic constants of C_{N2}@gh-C₃N₄ sheets satisfy all the criteria to be mechanically stable. Young's modulus (Y) and Poisson's ratio (PR) are calculated using the following formulas.³

$$Y = (C_{11}^2 - C_{12}^2) / C_{11} \quad (6)$$

$$PR = C_{12} / C_{11} \quad (7)$$

Table S3: Exchange energy (E_{ex}) and Curie temperature (T_C) value of 12.50% C_N@gh-C₃N₄ system.

Compound	Magnetic Moment/ C (μ_B)	Exchange energy (meV)/C [$E_{ex} = E_{FM} - E_{AFM}$]	Energy Difference (meV)/C ($E_{diff} = E_{FM} - E_{NSP}$)	Curie Temperature (T_C) in (K)	MAE in (μeV)/C (Magnetic Anisotropy Energy)
$C_{N1}@gh-C_3N_4$	0.90	-111.41	-47.89	294	9.83
$C_{N2}@gh-C_3N_4$	1.00	-151.54	-30.26	402	12.20
$C_{N3}@gh-C_3N_4$	0.80	-75.53	-22.31	204	7.36

Text S3. Calculation of Magnetic Anisotropy Energy (MAE)

The magnetic anisotropy energy (MAE) is calculated by applying the torque approach.⁷⁻⁸ Non-collinear self-consistent calculations (including spin orbit coupling) are performed in the z, y and x axis magnetization directions, respectively. MAE originates from the perpendicular and in plane contribution of spin orbit coupling (SOC), which can be expressed in terms of angular momentum operators L_x , L_y or L_z . So the contribution of different spins (up ‘ $\uparrow\uparrow$ ’ and down ‘ $\downarrow\downarrow$ ’) can be expressed by the second order perturbation equation.⁶

$$MAE = \xi^2 \sum_{o,u} \frac{|\langle o | L_Z | u \rangle|^2 - |\langle o | L_X | u \rangle|^2}{E_u - E_o}$$

Here, o and u represent the occupied and unoccupied electronic states, respectively. The E_o and E_u in the denominator are their respective band energies. L_Z and L_X are the angular momentum operators along Z and X axis, and ξ denotes the strength of the SOC. So, a potential with good MAE for practical application should hold a high value of ξ . Then, the MAE is calculated using the following equation:

$$MAE = E_{S0} - E_{S1} \quad (8)$$

Where E_{S0} is the energy of the materials without employing any magnetic axis and E_{S1} is the energy in presence of an easy axis. Total energies are converged to a precision of 10^{-6} eV in MAE calculations.

Text S3.1 Mean Field Theory (MFT):

We have taken the MFT approach to calculate the Curie temperature for the two dimensional $C_N@gh-C_3N_4$ systems. This method has been previously used by Li et al.⁹ for the Curie temperature calculation for Mn-phthalocyanine (MnPc) system. The main idea behind MFT method is to replace all interactions to any one body with an average or effective interaction.¹⁰ It reduces any multi-body problem into an effective one-body problem. The detailed partition function can be written as follows,

$$Z = \sum_{m=-M, -M+2, \dots, M-2, M} e^{\gamma J' m \langle M \rangle / k_B T} \quad (9)$$

Here, ‘ J' ’ is the exchange parameter, ‘ γ ’ is the coordination number, ‘ m ’ is the ensemble-average magnetic moment, and ‘ M ’ is the calculated magnetic moment of the system.

Thus, the average spin of each magnet becomes,

$$\langle m \rangle = \frac{1}{Z} \sum_{m=-M, -M+2, \dots, M-2, M} m \times e^{\gamma J' m \langle M \rangle / k_B T} \quad (10)$$

Now, if we assume that, $P = \frac{\gamma J'}{k_B T}$, then the equation 5 becomes,

The above equation can be easily deducible when the parameter ‘ P ’ varies along with the static solution $\langle m \rangle$. At the critical point,

$$P = P_c = \frac{\gamma J'}{k_B T_c} \quad (11)$$

At this critical point, the phase transition of the system between ferromagnetic to paramagnetic occurs. This critical point is known as Curie temperature.

3.2 Monte Carlo Simulations:

Monte Carlo simulations involve generating a subset of configurations or samples, chosen using a random algorithm from a configuration space, according to a probability distribution or weight function. Observables are then computed as averages over the samples.¹¹

One sample or configuration of the magnet is a particular assignment of spin values, say

$$s_1 = +1; s_2 = -1; s_3 = +1; \dots \dots \dots ; s_{N_s} = +1 \quad (12)$$

in which each spin is set “up” or “down”. According to statistical mechanics, the average value of an observable is got by weighting each configuration with the Boltzmann factor. For example, the average magnetization at some fixed temperature T is given by,

$$\langle M \rangle = \frac{\sum_{config} M e^{-E/k_B T}}{\sum_{config} e^{-E/k_B T}} \quad (13)$$

At the Curie temperature (T_c) we expect a marked fluctuation in the magnetic moment (M).

Reference:

- [1] M. Topsakal, S. Ciraci, *Phys. Rev. B: Condens. Matter Mater. Phys.* 2010, **81**, 024107.
- [2] S. Zhang, J. Zhou, Q. Wang, C. Xiaoshuang, K. Yoshiyuki, P. Jena. *Proc. Natl. Acad. Sci. U.S.A.* 2015, **112**, 2372.
- [3] J. M. de Sousa, T. Botari, E. Perim, R. A. Bizaio, D. S. Galvao, arXiv:1606.01055v1
- [4] R. C. Andrew, R. E. Mapasha, A. M. Ukpong, and N. Chetty. *Phys. Rev. B* 2012, **85**, 125428.
- [5] K. Wright, J. D. Gale. *Phys. Rev B* 2004, **70**, 035211.
- [6] Y. Ding, Y. *J. Phys. Chem. C* 2013, **117**, 18266–18278.
- [7] J. Hu; R. Wu, *Phys. Rev. Lett.*, 2013, **110**, 097202.
- [8] D. S. Wang, R. Q. Wu, A. J. Freeman, *Phys. Rev. B: Condens. Matter Mater. Phys.*, 1993, **47**, 14932.
- [9] X. Li, X. Wu, J. Yang. *J. Am. Chem. Soc.* 2014, **136**, 5664.

[10] P. M. Chaikin, T. C. Lubensky, (2007). Principles of condensed matter physics (4th print ed.). Cambridge: Cambridge University Press. ISBN 978-0-521-79450-3.

[11] D. P. Kroese, T. Brereton, T. Taimre, Z. I. Botev, *Comput. Stat.* 2014, **6**, 386.